Journal of Materials Chemistry A

COMMUNICATION

View Article Online
View Journal | View Issue

Cite this: J. Mater. Chem. A, 2017, 5, 6032

Received 9th January 2017
Accepted 6th March 2017

DOI: 10.1039/c7ta00248c

rsc.li/materials-a

A coaxial triboelectric nanogenerator fiber for energy harvesting and sensing under deformation†

Xinghai Yu,‡ Jian Pan,‡ Jing Zhang, Hao Sun, Sisi He, Longbin Qiu, Huiqing Lou, Xuemei Sun* and Huisheng Peng*

A novel coaxial triboelectric nanogenerator fiber for both energy harvesting and sensing under deformation was developed by using aligned carbon nanotube sheets as inner and outer electrodes and designing porous structures in triboelectric polymers of polydimethylsiloxane and polymethyl methacrylate. The fiber device was flexible, stretchable, weavable and adaptable for integration with various other electronic devices. Besides the capability of converting multidirectional mechanical energies to electricity with a high durability, it can also sense diverse mechanical stimuli such as pressing, bending, twisting, stretching and vibrating.

Harvesting renewable and sustainable energy from an ambient environment has been considered as one of the most effective approaches to meet the tremendous energy consumption in modern society.[1–4] Recently, with the emergence of wearable electronics, harvesting mechanical energy from human movements to power these electronic devices has attracted increasing attention. To this end, a surprising number of mechanical energy harvesting devices based on piezoelectricity,[5–7] triboelectrification[8–11] and electrostatic induction[12–14] have been developed. Among them, triboelectric nanogenerators are extensively studied due to their simple fabrication, low cost, various structures and high output performance. However, most triboelectric nanogenerators appear in planar or strip structures, which are difficult for integration and adaptation to human motions in diverse directions to meet the requirements of portable and wearable electronics.[15–18] One-dimensional triboelectric nanogenerators such as a fiber that can be efficiently integrated with other electronic devices and woven into lightweight fabrics are thus highly desired. In particular, they are promising to operate under multidirectional forces so as to harvest various mechanical energies in real life.

Several attempts have thus been made to fabricate fiber-shaped triboelectric nanogenerators (FTENGs) typically by assembling two triboelectric fibers together in a parallel structure or with the overlap of fabric.[19–21] Through sequential contact–separation between the two fibers with different polarities of triboelectricity under mechanical force, the electric output was generated continuously. The assembled structure is prone to cracking, because the two fibers would fall apart from each other during the practical use with complex deformations and mechanical stresses from different directions. To this end, a coaxial structure would be a more favorable candidate,[22] which has been widely applied for other fiber-shaped energy harvesting and storage devices such as solar cells,[23] supercapacitors,[24] and lithium-ion batteries.[25,26] Compared to the two-fiber-twisted structure, the coaxial structure showed a higher stability under various deformations especially bending and stretching. In addition, the reported FTENGs are mainly based on metal electrodes under a vertical-separation contact mode, which may restrict the flexibility while increasing the complexity of fabrication and the weight. It remains challenging to achieve flexible, lightweight, stable and sensitive FTENGs with a coaxial structure for efficient mechanical energy harvesting.

Here we demonstrate a novel coaxial triboelectric nanogenerator fiber (CTNF) with high performance. The fiber device was fabricated from a polydimethylsiloxane (PDMS) fiber substrate; two multi-layer aligned carbon nanotube (CNT) sheets served as inner and outer electrodes and PDMS and polymethyl methacrylate (PMMA) were used as contact materials for triboelectrification. To enhance the output performance, we designed microstructured surfaces on both PDMS and PMMA to largely increase the roughness and contact for generating more charges. In addition, an air gap was employed for effective contact and separation of the triboelectric materials. The CTNF was flexible, stretchable, weavable and adaptable for integration with various other electronic devices. Besides the capability of converting

State Key Laboratory of Molecular Engineering of Polymers, Department of Macromolecular Science, Laboratory of Advanced Materials, Fudan University, Shanghai 200438, China. E-mail: sunxm@fudan.edu.cn; penghs@fudan.edu.cn

† Electronic supplementary information (ESI) available. See DOI: 10.1039/c7ta00248c

‡ These authors contributed equally to this work.

multidirectional mechanical energies to electricity, it can also sense diverse mechanical stimuli such as pressing, bending, twisting, stretching and vibrating.

Fig. 1a schematically shows the structure of the CTNF with the fabrication details in Fig. S1–S3.† Briefly, PMMA microspheres were first deposited onto the inner layer of aligned CNT sheets that had been wrapped on the pre-stretched PDMS fiber substrate. Sucrose particles were then subsequently dip-coated onto the resulting fiber and further coated with PDMS. After curing, the sucrose particles, the sacrificial layer, were dissolved to generate an air gap between PMMA and PDMS and pores on the surface of the PDMS layer to increase the roughness. Finally, the outer layer of aligned CNT sheets was wrapped and packaged with another PDMS layer to form the CTNF. Fig. 1b and c show the scanning electron microscopy (SEM) images of the cross section of a CTNF with the air gap of ~10 μm. The PMMA microspheres with a diameter of 0.5 μm were assembled into a uniform layer with a thickness of ~20 μm (Fig. 1c and d). A lot of pores with an average size of nearly 5 μm were created on the inner side of PDMS (Fig. 1e). As expected, the CTNF could be deformed into various patterns such as a knot (Fig. 1f) and a textile (Fig. 1g).

The energy harvesting mechanism of the CTNF is schematically illustrated in Fig. 2. At the original state, there were no charges on both the PMMA microspheres and the porous PDMS layer. When the CTNF was deformed under an external force, the two polymer layers came into contact with each other, and the electrons on the surface of PMMA would transfer to the PDMS layer to generate triboelectric positive and negative charges on their surfaces, respectively (Fig. 2a).[27–29] Due to the insulation of both PMMA and PDMS, the generated positive and negative charges were effectively maintained. Therefore, an electric potential difference was established between the two layers when they separated after the removal of the external force (Fig. 2b). The electrons would flow from the outer CNT sheet electrode with a low potential to the inner electrode with a high potential through the external circuit to reach equilibrium (Fig. 2c), resulting in a positive current output. When the CTNF was deformed again and the two layers got close to each other, the positive potential difference formed between PDMS and PMMA would cause the electrons to flow back from the

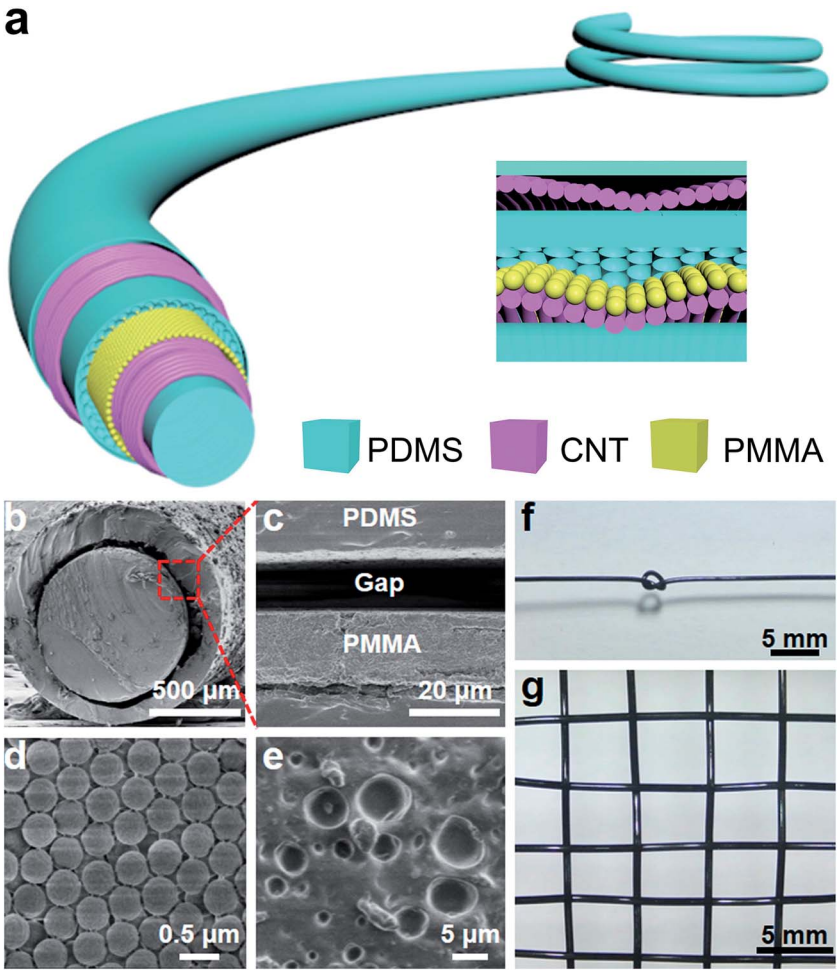

Fig. 1 The structure, flexibility and weavability of the CTNF. (a) A schematic diagram. (b) and (c) Cross-sectional SEM images at low and high magnifications, respectively. (d) PMMA microspheres with a diameter of 0.5 μm deposited on aligned CNT sheets. (e) PDMS layer with a porous structure. (f) and (g) Photographs of the CTNF being tied into a knot and woven into a textile, respectively.

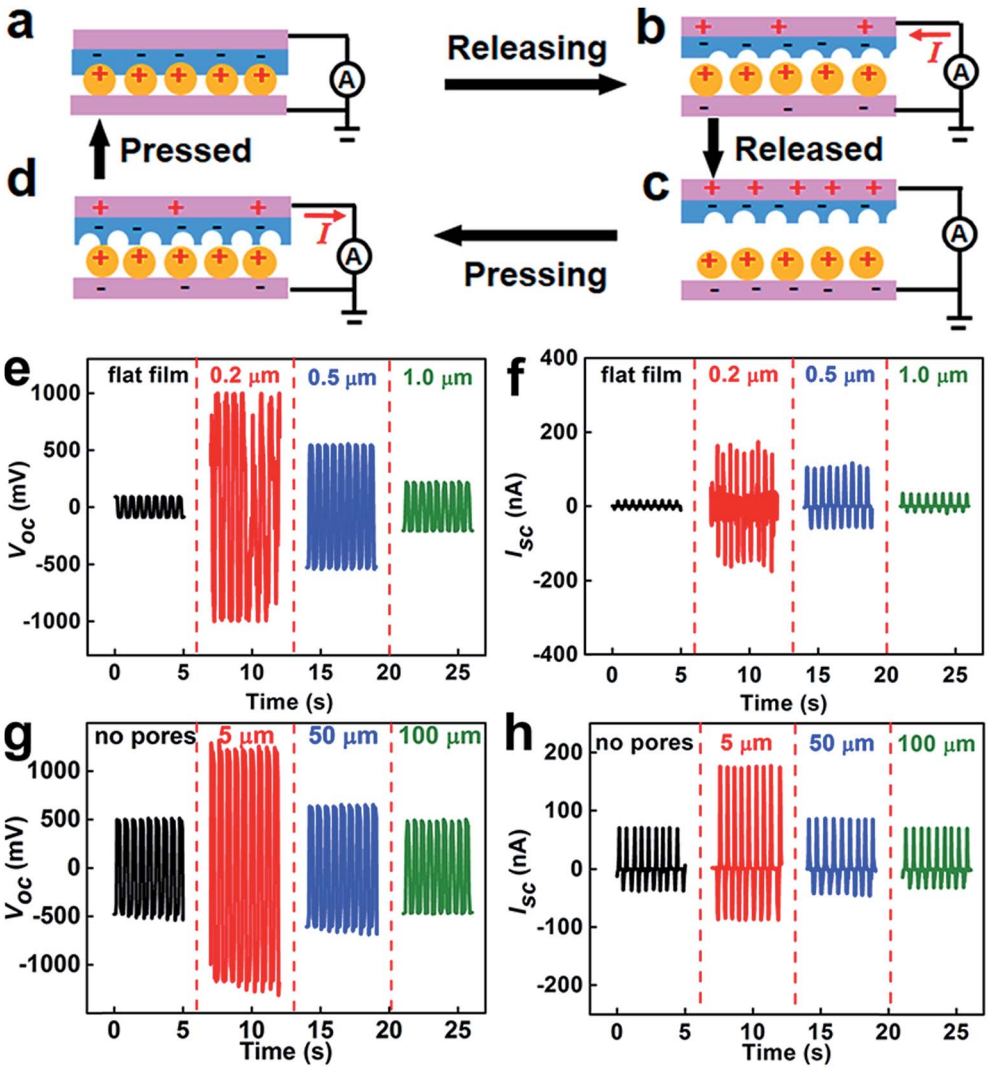

Fig. 2 The working mechanism and output performance of the CTNF. (a–d) Schematic diagrams of the CTNF being fully pressed, during releasing, fully released and during pressing, respectively. (e) and (f) Open-circuit voltage (V_{oc}) and short-circuit current (I_{sc}) without and with different sizes of PMMA microspheres, respectively. (g) and (h) V_{oc} and I_{sc} without and with porous structures of different sizes, respectively. The length of the CTNF was 2.5 cm, and the tests were performed under a pressing force of 10 N.

inner electrode to the outer electrode (Fig. 2d). This process generated a negative electric signal until reaching the second equilibrium with the two layers in contact again (Fig. 2a). Therefore, with the repeated contact and separation of the two polymer layers under a periodic external force of 25 N, the CTNF of approximately 5 cm in length generated an alternating electric output with the open-circuit voltage (V_{oc}) of nearly 5 V and a short-circuit current (I_{sc}) of 240 nA (Fig. S4 and S5†), respectively.

The amount of charges on the surface induced by the triboelectric effect was greatly dependent on the surface area of the PMMA and PDMS layers. Therefore, microstructures with a larger surface area were important for the high performance of the CTNF. For the PMMA, microspheres were deposited to form a uniform layer. Under a vertical pressing force of 10 N, a 2.5 cm-long CTNF derived from PMMA microspheres with a diameter of 200 nm output a V_{oc} of 1 V and a I_{sc} of 150 nA, which were about 8 and 6 fold that of the one based on PMMA film without microspheres (Fig. 2e and f). However, the output performance decreased when the diameter of PMMA microspheres was further increased to 500 nm and 1.0 μm due to decreasing surface area. In addition, the larger microspheres were difficult to form into a uniform layer and produced defects and vacancies in the PMMA layer, which further reduced the effective contact surface for charge induction (Fig. S6†).

The PDMS layer was modified with a porous structure on the inner surface by introducing sacrificial sucrose particles (Fig. S7†). Without pores, the CTNF showed a V_{oc} of 500 mV and a I_{sc} of 75 nA. For the inner pores with an average size of nearly 5 μm, the output V_{oc} and I_{sc} were enhanced by 150% and 130% respectively (Fig. 2g and h). However, when the size of the inner pores was further increased to 50 and 100 μm, the output performance of the CTNF reduced obviously due to decreasing roughness and contact area. Besides, the output performance of

the CTNF was also influenced by the spacing between the two contact layers (Fig. S8†). For instance, a spacing of 10 μm was typically used in CTNFs. When the spacing was decreased, *e.g.*, to 5 μm, the output current decreased, possibly due to the reduced electrostatic induction of charges on the electrodes. When the spacing was increased to a larger distance of 20 μm, it would take a longer time for the two layers to come into contact and separate, thus reducing the efficiency of charge flow and decreasing the output electric signals.[30]

In real life, mechanical energy can be generated from a variety of deformations besides normal pressing such as bending, twisting, stretching and vibrating. In this CTNF, PDMS was the main component providing flexibility and stretchability; the aligned CNT sheet electrodes also enabled high conductivity and stability under deformation, and the PMMA layer from the assembled microspheres contributed to good triboelectric properties with porous PDMS. Therefore, the CTNF could deform in various modes to harvest energy. Fig. 3 presents the output signals of a CTNF under various deformations. When the CTNF was bent and twisted, a similar V_{oc} of ~600 mV was generated (Fig. 3a and b). Under repeated stretching and releasing, the CTNF exhibited a maximal V_{oc} of 1.1 V (Fig. 3c). A shockwave of the output signal was also obtained upon the vibration of the CTNF plucked by a finger (Fig. 3d and S9†). During a damped vibration, the CTNF produced a V_{oc} of 500 mV at the very beginning which then decreased with reducing amplitude of the fiber. Therefore, the CTNF was capable of harvesting mechanical energy from diverse directions during operation and converting it into electric energy efficiently. In addition, the CTNF was operated repeatedly under pressing

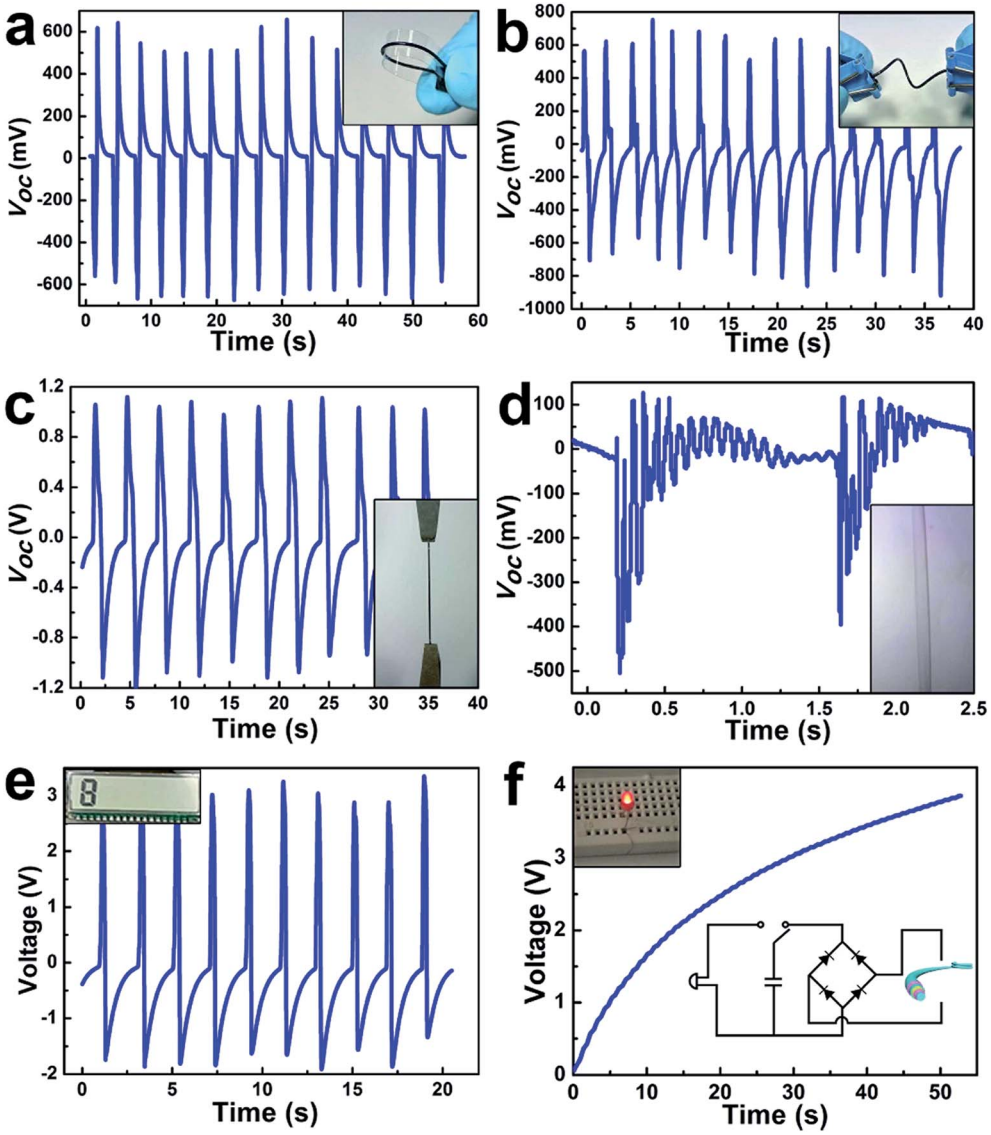

Fig. 3 The open-circuit voltages (V_{oc}) of the CTNF generated under (a) bending, (b) twisting, (c) stretching and (d) vibrating; the insets show the corresponding states of different deformations. (e) The output voltage of the CTNF under pressing (the inset, an LCD being lit by the CTNF). (f) The rectified voltage of the CTNF to charge a capacitor (the top left inset, an LED being lit by the charged capacitor; the right bottom inset, the circuit diagram).

(Fig. S10†) and bending (Fig. S11†) for over 2000 and 8000 cycles, respectively, and the performance remained almost unchanged, indicating a high durability. For practical application, the influence of moisture, temperature and washing was then tested. The voltage decreased with increasing humidity (Fig. S12†) while it changed little with temperature (Fig. S13†). After washing, no significant change was observed in the output performance of the CTNF (Fig. S14†).

The energy harvested by the CTNF could be used to charge capacitors and light up liquid crystal displays (LCDs) and light emitting diodes (LEDs). For example, a commercial LCD could be lit up to display the number "8" by pressing a CTNF (Fig. 3e). The electric energy generated by four CTNFs connected in parallel was rectified (Fig. S15†) to charge a commercial capacitor (22 μF), with the voltage reaching ~3.8 V within 50 s (Fig. 3f). The fully charged capacitor could light a commercial LED.

As the CTNFs could generate electric signals under deformation, they could in turn be used as sensors for physiological motion capture, health care and human–machine interaction. The I_{sc} values had been enhanced with increasing pressing forces (Fig. S16a†). No obvious changes were found under increasing frequencies from 0.1 Hz to 0.5 Hz at the same force of ~25 N (Fig. S16b†). Since human activities mainly occur at the low-frequency regime (<1 Hz),[31] the CTNFs are promising for wearable sensors to distinguish the subtle activities of vegetative patients for health care or human–machine interaction. For instance, the CTNF was capable of detecting the finger joint motion (Fig. 4a). Four CTNFs had been fastened on four fingers and connected in parallel, and electric signals were generated when any finger was bent and released. A V_{oc} of ~400 mV was produced for one bent finger. When the number of bent fingers was increased from one to two, three and four, the generated electric signals also increased in proportion.

Besides the wearable field, the CTNF can also play a role in other detections, for example, tracking the movement of animals and objects in a definite area by their velocity and direction. Here, a toy car was used to show the usability of the fiber detector. The experiments were performed by suspending a CTNF above a round lane as a touch sensor. When a toy car was run on the round lane with a certain velocity and passed the CTNF sensor repeatedly, electric signals were generated periodically (Fig. 4b). The calculated velocities from the detection showed relative deviations of 0.56%, 0, 0.56%, 1.1% and 1.1% for five samples (Fig. 4c, Text S1 and Table S1†), which indicated an accurate and credible measurement. Additionally, the moving direction of the car could be detected by using two different CTNFs (Fig. S17†). We put a short and a long CTNF at points A and B, respectively. When the car moved in the clockwise direction, the CTNFs A and B deformed successively and produced superimposed electric signals with two positive peaks showing a difference of ~0.35 V. In the anticlockwise cycle, the car touched the CTNF B first and then A, generating a larger difference of ~0.70 V between the two peaks. Therefore, the CTNFs could be used to detect the moving direction according to the voltage difference.

In summary, a new family of coaxial triboelectric nanogenerator fibers was developed by designing porous structures in

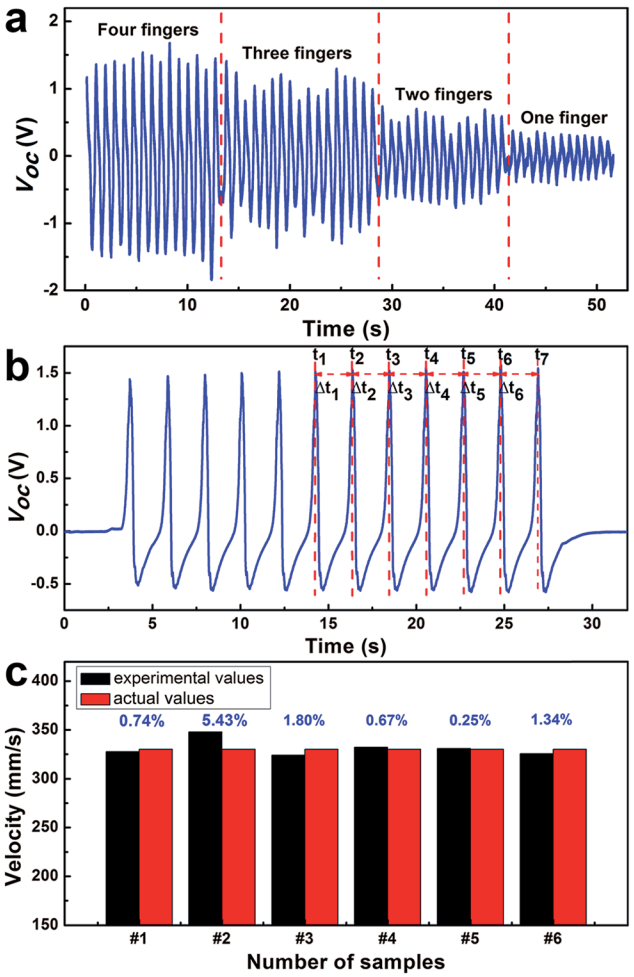

Fig. 4 The application of the CTNF for the detection of the finger motion and moving velocity. (a) The voltages of the CTNF working as a motion-capturing sensor to detect the bending of fingers. (b) The open-circuit voltages for calculating the velocity of a car. (c) The relative deviations of five detections.

triboelectric polymers and using aligned CNT sheets as electrodes. These soft materials, in contrast to conventionally used metals or metal oxides, reduced the weight while increasing the flexibility and stability of the fiber devices. The capability to harvest diverse mechanical energies makes the CTNFs competent to serve as a power supply source. Moreover, their response to a variety of mechanical stimuli, including bending, vibrating, stretching and twisting, afforded the sensing capacity of the CTNF, for instance, to monitor the motions of finger joints and detect the velocity and direction of a moving car. These remarkable merits revealed the great prospects of the CTNF particularly in intelligent electronics, such as personal healthcare, traffic tracking and velocity detection.

Acknowledgements

This work was supported by the NSFC (21634003, 51573027, 51403038, and 51673043), MOST (2016YFA0203302) and STCSM (16JC1400702, 15XD1500400, and 15JC1490200).

Notes and references

1 S. Chu and A. Majumdar, *Nature*, 2012, **488**, 294–303.
2 D. Larcher and J. Tarascon, *Nat. Chem.*, 2015, **7**, 19–29.
3 X. Yuan, X. Liu and J. Zuo, *Renewable Sustainable Energy Rev.*, 2015, **42**, 298–305.
4 Z. Song and H. Zhou, *Energy Environ. Sci.*, 2013, **6**, 2280–2301.
5 X. Li, Z. Lin, G. Cheng, X. Wen, Y. Liu, S. Niu and Z. L. Wang, *ACS Nano*, 2014, **8**, 10674–10681.
6 M. Lee, C. Chen, S. Wang, S. Cha, Y. Park, J. Kim, L. Chou and Z. L. Wang, *Adv. Mater.*, 2012, **24**, 1759–1764.
7 J. Lee, K. Lee, B. Kumar, T. Thanh, N. Lee and S. Kim, *Energy Environ. Sci.*, 2013, **6**, 169–175.
8 C. Wu, T. Kim, F. Li and T. Guo, *ACS Nano*, 2016, **10**, 6449–6457.
9 S. Jung, J. Lee, T. Hyeon, M. Lee and D. Kim, *Adv. Mater.*, 2014, **26**, 6329–6334.
10 K. Zhang, Z. L. Wang and Y. Yang, *ACS Nano*, 2016, **10**, 4728–4734.
11 G. Wang, Y. Xi, H. Xuan, R. Liu, X. Chen and L. Cheng, *Nano Energy*, 2015, **18**, 28–36.
12 J. Zhong, Q. Zhong, Q. Hu, N. Wu, W. Li, B. Wang, B. Hu and J. Zhou, *Adv. Funct. Mater.*, 2015, **25**, 1798–1803.
13 J. Zhong, Y. Zhang, Q. Zhong, Q. Hu, B. Hu, Z. L. Wang and J. Zhou, *ACS Nano*, 2014, **8**, 6273–6280.
14 X. Yu, J. Pan, J. Deng, J. Zhou, X. Sun and H. Peng, *Adv. Mater.*, 2016, **28**, 10744–10749.
15 S. Wang, L. Lin and Z. L. Wang, *Nano Lett.*, 2012, **12**, 6339–6346.
16 K. Lee, J. Chun, K. Kim, M. Kim, M. Gupta and J. Baik, *Adv. Mater.*, 2014, **26**, 5037–5042.
17 S. Wang, Y. Zi, Y. Zhou, S. Li, F. Fan, L. Lin and Z. L. Wang, *J. Mater. Chem. A*, 2016, **4**, 3728–3734.
18 L. Liu, J. Pan, P. Chen, J. Zhang, X. Yu, X. Ding, B. Wang, X. Sun and H. Peng, *J. Mater. Chem. A*, 2016, **4**, 6077–6083.
19 J. Wang, X. Li, Y. Zi, S. Wang, Z. Li, L. Zheng, F. Yi, S. Li and Z. L. Wang, *Adv. Mater.*, 2015, **27**, 4830–4836.
20 W. Seung, M. Gupta, K. Lee, K. Shin, J. Lee, T. Kim, S. Kim, J. Lin, J. Kim and S. Kim, *ACS Nano*, 2015, **9**, 3501–3509.
21 X. Pu, L. Li, H. Song, C. Du, Z. Zhao, C. Jiang, G. Cao, W. Hu and Z. L. Wang, *Adv. Mater.*, 2015, **27**, 2472–2478.
22 K. Kim, J. Chun, J. Kim, K. Lee, J. Park, S. Kim, Z. L. Wang and J. Baik, *ACS Nano*, 2015, **9**, 6394–6400.
23 L. Qiu, J. Deng, X. Lu, Z. Yang and H. Peng, *Angew. Chem., Int. Ed.*, 2014, **53**, 10425–10428.
24 X. Chen, L. Qiu, J. Ren, G. Guan, H. Lin, Z. Zhang, P. Chen, Y. Wang and H. Peng, *Adv. Mater.*, 2013, **25**, 6436–6441.
25 W. Weng, Q. Sun, Y. Zhang, H. Lin, J. Ren, X. Lu, M. Wang and H. Peng, *Nano Lett.*, 2014, **14**, 3432–3438.
26 Y. Zhang, L. Wang, Z. Guo, Y. Xu, Y. Wang and H. Peng, *Angew. Chem., Int. Ed.*, 2016, **55**, 4487–4491.
27 A. Diaz and R. Felix-Navarro, *J. Electrost.*, 2004, **62**, 277–290.
28 L. McCarty and G. Whitesides, *Angew. Chem., Int. Ed.*, 2008, **47**, 2188–2207.
29 B. Meng, W. Tang, Z. Too, X. Zhang, M. Han, W. Liu and H. Zhang, *Energy Environ. Sci.*, 2013, **6**, 3235–3240.
30 G. Zhu, Z. Lin, Q. Jing, P. Bai, C. Pan, Y. Yang, Y. Zhou and Z. L. Wang, *Nano Lett.*, 2013, **13**, 847–853.
31 P. Turnbaugh, R. Ley, M. Mahowald, V. Magrini, E. Mardis and J. Gordon, *Nature*, 2006, **444**, 1027–1031.